Arch. Metall. Mater. **70** (2025), 4, 1883-1896

DOI: https://doi.org/10.24425/amm.2025.156275

B. IMANE[1,2,3], N. LABJAR[1*], M. KADDAMI[2], M. ESSAHLI[3], L. EL MOSTAPHA[3], A. DAHROUCH[4], S. EL HAJJAJI[5]

MICROSTRUCTURE AND SURFACE DEGRADATION OF Al-Al_9Co_2-$Al_{13}Co_4$ COMPOSITES IN HCl MEDIUM

The Al-Co alloys corrosion resistance of various Co compositions (0.5-5 at.% Co) at different sintering times (4 h, 8 h, 24 h, 48 h, and 72 h) for 25°C in (1M) hydrochloric acid electrolyte was studied by employing the electrochemical impedance spectroscopy (EIS) and the tafel polarization. Raman technique was used to identify the surface film of aluminum and its alloys, and scanning electron microscope (SEM) coupled with energy-dispersive X-ray spectroscopy (EDS) was used to determine the microstructure of the materials. In comparison to undoped aluminum, the Al-5 at.% Co material sintered at forty-eight hours exhibited outstanding corrosion performance. Pitting is discernible in the microstructure of sintered materials, particularly within the Al_9Co_2 phase. This phase exhibits faster corrosion compared to other intermetallic compounds such as $Al_{13}Co_4$. In terms of crystal structure and chemical composition of the dopant, the Al-Co intermetallic compounds are classed as a function of their relative nobility.

Keywords: Al-Co alloys; Corrosion Test; Complex Metal Alloys; Microstructure; Raman Spectroscopy; Phase Equilibrium

1. Introduction

Aluminum ranks as the second most appealing material after iron, owing to its extensive use in many industrial areas [2-11-13]. This interest potential is primarily attributable to its density to weight and resistance to weight ratios, electrical and thermal conductivity, weldability, non-toxicity, stability at low temperatures, reflectivity, toughness, formability, resistance to impacts, corrosion resistance, low price, and recyclable nature [1,2,3,4,5-11-13-29]. In order to enhance the properties of aluminum to meet the requirements of industrial technical applications.

Researchers have recently become very interested in the doping of aluminum with 'TM' transition metals (Co, Ti, Ni, Cu, Zn… etc.) because they combine good mechanical and physical properties, high melting temperatures, and low density. By altering the heat treatment conditions of these Al-TMs supersaturated solid solutions, disordered alloys, quasicrystals, ordered intermetallic compounds, and complex metal alloys (CMAs) can all be created [9]. In particular, Al-Co alloys are a component of this new class of complex metal alloys (CMAs) [6-22]. In contrast to conventional metal alloys, the latter materials have desirable physical features [6,7-30].

Studies on the corrosion of aluminum are required because of the fact that these alloys are frequently used in industry and can seriously deteriorate in harsh environments [10-12-23]. Aluminum corrosion resistance significantly declines, which causes surface structural degradation issues such as pitting, cracks, fractures, intergranular degeneration, and failures. Undoped aluminum's key characteristic, which is the presence of an inert, protective, invisible oxide film clinging to the metal surface, provides it with adequate corrosion resistance [5-13-24]. However, because of its amphoteric nature [2-11-13], this passive film is quickly degraded when exposed to hostile environments. In particular, their dissolution in acids might result in the creation of Al^{3+} ions [13].

Strong acids like hydrochloric acid (HCl) are frequently used in electropolishing, chemical and electrochemical grafting, pickling, and cleaning aluminum surfaces to remove dust and scale before some industrial processes including galvanizing

[1] MOHAMMED V UNIVERSITY IN RABAT, LABORATORY OF SPECTROSCOPY, MOLECULAR MODELING, MATERIALS, NANOMATERIALS, WATER AND ENVIRONMENT, CERNE2D, ENSAM, RABAT, MOROCCO
[2] HASSAN FIRST UNIVERSITY OF SETTAT, FACULTY OF SCIENCE AND TECHNOLOGY, LABORATORY OF RESEARCH: PHYSICAL-CHEMISTRY OF PROCESSES AND MATERIALS, SETTAT, 26000, MOROCCO
[3] HASSAN FIRST UNIVERSITY OF SETTAT, FACULTY OF SCIENCE AND TECHNOLOGY, LABORATORY OF RESEARCH: APPLIED CHEMISTRY AND ENVIRONMENT, SETTAT, 26000, MOROCCO
[4] INSTITUT DE CRIMINALISTIQUE DE LA GENDARMERIE ROYALE, RABAT, MOROCCO
[5] MOHAMMED V UNIVERSITY IN RABAT, LABORATORY OF SPECTROSCOPY, MOLECULAR MODELING, MATERIALS, NANOMATERIALS, WATER AND ENVIRONMENT, CERNE2D, FACULTY OF SCIENCES, RABAT, MOROCCO

* Corresponding author: najoua.labjar@ensam.um5.ac.ma

and hot dip coating [5-11-13]. However, it causes strong corrosion (pitting) on aluminum when it comes into contact with chlorides [11-13]. Because the development of industrial applications relies heavily on corrosive behavior. Controlling the corrosion of aluminum in various conditions is crucial. Numerous techniques, including anodizing, coatings, the inclusion of various alloying elements, and the use of inhibitors, have been suggested in this sense [2-11].

Our recent study examines the impact of heat treatment variables, such as sintering time and cobalt content, on the microstructural morphology, structural change, and mechanical behavior of Al-Al_9Co_2-$Al_{13}Co_4$ composites [25]. The Al-Co alloy's corrosion performance is a subject of very little research [6,7]. Aluminum can be strengthened such that it is more responsive to the electrochemical action of chloride environment, the current study improves aluminum corrosion performance in an acidic medium (1M) HCl [2]. This work aims to assess the electrochemical behavior of aluminum (Al) reinforced with intermetallic compounds Al_9Co_2 and $Al_{13}Co_4$. Based on the phase equilibrium diagram [26] and several thermal treatment periods ranging from 4 hours to 72 hours, we experimented with low Co compositions (0.5, 1, 3, and 5 at.% Co) to achieve this objective. On the one hand, the ideal conditions (Cobalt composition and thermal treatment time) that could provide a good corrosion performance have been determined. The price of the base metals required to create these composites should be reduced [25].

2. Materials and methods

2.1. Electrochemical Testing

The specimens used in the current work were made of undoped Al and Al-x at.% Co alloys with x = 0.5, 1, 3, and 5 at.% Co. In our study mentioned above [25], the development of all materials was reported in detail. They were prepared by applying the 'SFS' solid phase sintering process under an N_2 atmosphere for many thermal treatment times from 4 hours to 72 hours at the temperature of 600°C. We have chosen to advance materials development by employing extended heat treatment times. This approach aims to achieve two primary objectives: first, to attain densification and thorough consolidation, and second, to minimize residual porosity in the developed materials as much as possible [32,33]. Hence, the heat treatment of these solid-state-prepared materials is conducted at various sintering times to optimize the parameters leading to the superior mechanical properties [25] and enhanced corrosion resistance. The materials listed below, are designated as 'SFS-0.5', 'SFS-1', 'SFS-3', and 'SFS-5'.

The potentiostat/galvanostat VMP_3 'BioLogic Science Instruments' was employed for studying undoped Al and its alloys corrosion in an acidic medium at several thermal treatment times. For that, a standard electrochemical cell is equipped with three electrodes. Platinum wire was carried out as the counter electrode, a reference electrode in silver chloride (AgCl) and to follow the progression of the reaction, we need to polarize the working electrode by using a potentiostat [30]. The scan rate of the reaction medium was 10 mV/s. The experiment of all samples was carried out in an acidic HCl (1M) environment [30].

After potential stabilization between –0.83 V and –0.7 V, the impedance measurement was applied, employing a 10 MV sinusoidal potential perturbation with frequencies between 100 kHz and 10 mHz [30].

The working electrode was given free reign to corrode before each experiment, and the open circuit potential (E_{OCP}) was measured as a function of time up to 30 minutes of immersion to produce a steady state of the E_{OCP}. For the good repeatability of our tests, each experience was made at least 3 rounds at 25°C [30].

2.2. Microstructural study

The surfaces of specimens were characterized by SEM-EDS (JEOL) working in the BSE mode with a tension of 20 kV [30].

2.3. Surface Characterisation

With the use of the Vertex 70 Bruker spectrometer (laser excitation wavelength of 514 nm, laser power of 12 mW, power incident on the sample surface of 2 mW, focused spot diameter of ~1 m) [30]. Raman Spectroscopy (TF) was used to examine the nature of the products deposited onto a 1cm diameter aluminum surface.

3. Results and Discussions

3.1. Static media

The mechanism of the dissolution reaction of aluminum in an acidic electrolyte may be written in terms of cathodic and anodic reactions [10].

$$H^+ + e^- \rightarrow 1/2H_2 \quad (1)$$

While the anodic reaction which results in the corrosion of aluminum is as followers :

$$Al + 3H^+ \rightarrow Al^{3+} \quad (2)$$

3.2. Microstructural Characterization of Sintered Materials

In our recently published research [25], we opted to develop Al-Al_9Co_2-$Al_{13}Co_4$ aluminum matrix composites by varying the cobalt composition (0.5, 1.3 and 5%) and the sintering time (4 h, 8 h, 24 h, 48 h, and 72 h) with the aim to enhance the mechanical properties of aluminum. We found that the microhardness of the

'SFS-5' composite increases as the sintering time extends from 4 hours to 24 hours. Nevertheless, beyond a sintering duration of 24 hours, the microhardness starts to decline with increasing sintering times. This result is proven by the exam an of the microstructure porosity in these composites. The porosity of the 'SFS-5' composite increases from 21.698±0.679 at a 24 h sintering time to 40.064±1.327 at a 72 h sintering time. This decrease in microhardness can be attributed to the Kirkendall phenomenon, which describes the formation of pores due to diffusion processes occurring during heat treatments [25].

3.3. Electrochemical Impedance Measurement

3.3.1. Potentiostatic Polarization Measurement

The Fig. 1 shows the Tafel plots for the undoped Al the'SFS-0.5', 'SFS-1', 'SFS-3', and 'SFS-5' materials in (1M) HCl electrolyte at 25°C.

The Tafel parameters as (E_{corr}) corrosion potential, (I_{corr}) corrosion current density, (β_a), (β_c) anodic and cathodic slopes, and 'R_p' polarization resistance are pooled in TABLE 1.

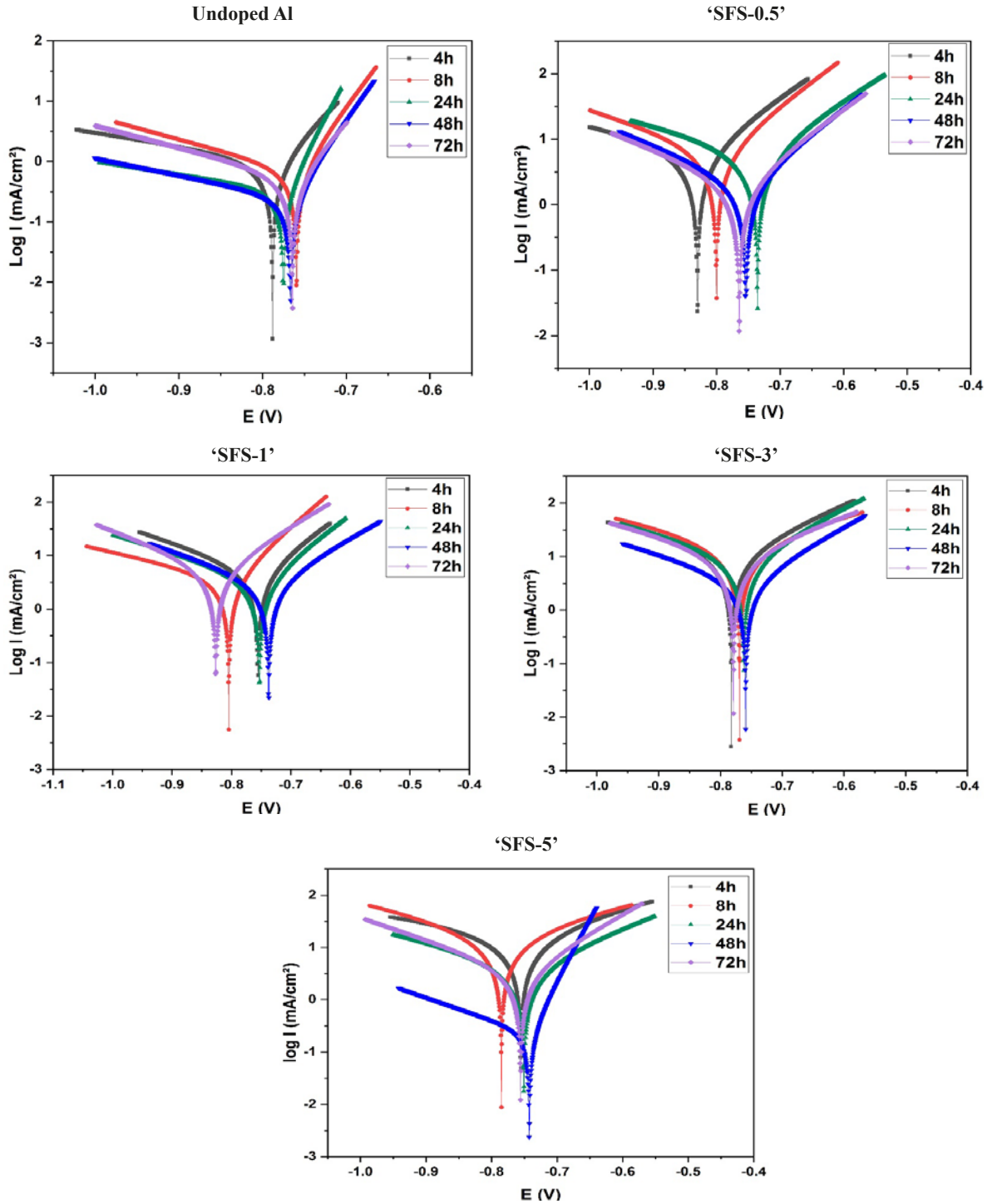

Fig. 1. Tafel plots of the undoped Al and the 'SFS-0.5', 'SFS-1', 'SFS-3', and 'SFS-5'materials in (1M) HCl electrolyte at various thermal treatment times

TABLE 1

Tafel parameters of the log $I = f(E)$ curves for the undoped Al and the SFS-0.5', 'SFS-1', 'SFS-3', and 'SFS-5'materials in (1M) HCl medium.

Specimens	Time	E_{corr} (V)	I_{corr} (mA.cm^{-2})	β_a(mV)	β_c(mV)	R_p
Undoped Al	4 h	–0.78	0.98	76.6	440.2	35.97
	8 h	–0.75	0.67	54.8	263.5	74.90
	24 h	–0.77	0.31	39.7	444.3	203.71
	48 h	–0.76	0.24	51.7	350.8	207.68
	72 h	–0.76	0.54	69.0	274.7	77.27
'SFS-0.5'	4 h	–0.83	6.57	157.2	441.5	3.02
	8 h	–0.79	4.42	111.1	234.2	6.90
	24 h	–0.73	4.17	133.4	283.5	6.08
	48 h	–0.75	2.74	152.4	312.4	8.17
	72 h	–0.76	2.59	162.0	317.1	8.27
'SFS-1'	4 h	–0.75	4.91	130.6	266.2	5.34
	8 h	–0.80	3.64	105.8	392.3	7.59
	24 h	–0.75	3.40	123.7	287.9	7.81
	48 h	–0.73	3.12	164.1	273.4	7.18
	72 h	–0.82	5.29	153.3	235.2	4.68
'SFS-3'	4 h	–0.78	19.73	288.9	396.3	0.69
	8 h	–0.76	19.46	346.0	438.7	0.61
	24 h	–0.76	8.07	164.7	288.2	2.72
	48 h	–0.74	4.74	204.5	659.5	3.11
	72 h	–0.77	11.50	254.4	345.4	1.36
'SFS-5'	4 h	–0.75	23.28	346.4	713.8	0.42
	8 h	–0.77	17.92	298.6	382.1	0.76
	24 h	–0.75	4.20	201.1	313.0	4.47
	48 h	–0.74	0.22	42.9	231.9	278.64
	72 h	–0.75	3.41	141.9	236.9	7.58

Fig. 2 shows the resistance polarization 'R_p' development for the undoped and the SFS-0.5', 'SFS-1', 'SFS-3', and 'SFS-5'materials for various thermal treatment times

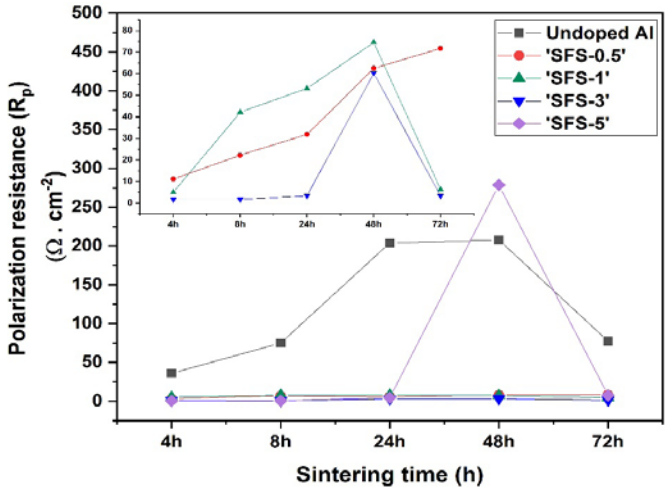

Fig. 2. Evolution of resistance polarization 'R_p' for the undoped Al and its alloys at various thermal treatment times in (1M) HCl electrolyte.

The polarization resistance evolution 'R_p' from the impedance spectroscopy concords well with the one obtained by the potentio-static polarization measurement.

The polarization resistance is calculated by the following equations:

$$R_p = \frac{\beta}{I_{corr}} \tag{3}$$

Where

$$\beta = \frac{2.303\left(\beta_a + \beta_c\right)}{\beta_a * \beta_c} \tag{4}$$

For the undoped Al, the time sintering had a good effect on corrosion performance as shown in (Figs. 1 and 2) and TABLE 1. It leads to the decrease of corrosion current density (I_{corr}) until 48h. Researchers have proven that undoped aluminum has a much lower (I_{corr}) and a more negative (E_{corr}) compared to the industrial aluminum. This is due to the presence of impurities such as Cu, Si, and Fe that result in the development of galvanic corrosion on the top of the aluminum surface [1].

Concerning the alloys, the corrosion resistance improved by the variation of the chemical composition of cobalt and the time sintering. It shows a lower corrosion density (I_{corr}) in the 'SFS-5' alloy treated at 48h than with the one found from the alloy produced by the sintering process or the alloys Al-28Co to Al-24Co studied by the author M. Palcut and his collaborators [6]. As a result, the environmental aggressiveness and the

variability of the metallurgical parameters such as a low Co composition as a function of the thermal treatment time. We were in a position to achieve a high electrochemical performance of these composites compared to a work published by Lekatou and his colleagues [18].

The solid solution of aluminum is less noble than the intermetallic compounds '$Al_{13}Co_4$' and 'Al_9Co_2' [6–18], as a result of the large gap in the standard potential of electrodes between the cobalt and aluminum [6]. And as will be shown in Section 3.5, the intermetallic compound $Al_{13}Co_4$ remains intact during polarization compared to Al_9Co_2 [6-18].

3.3.2. Nyquist diagrams

The Nyquist diagrams for undoped Al and the materials of 'SFS-0.5', 'SFS-1', 'SFS-3', and 'SFS-5' in (1M) HCl electrolyte at 25°C are displayed in Fig. 3.

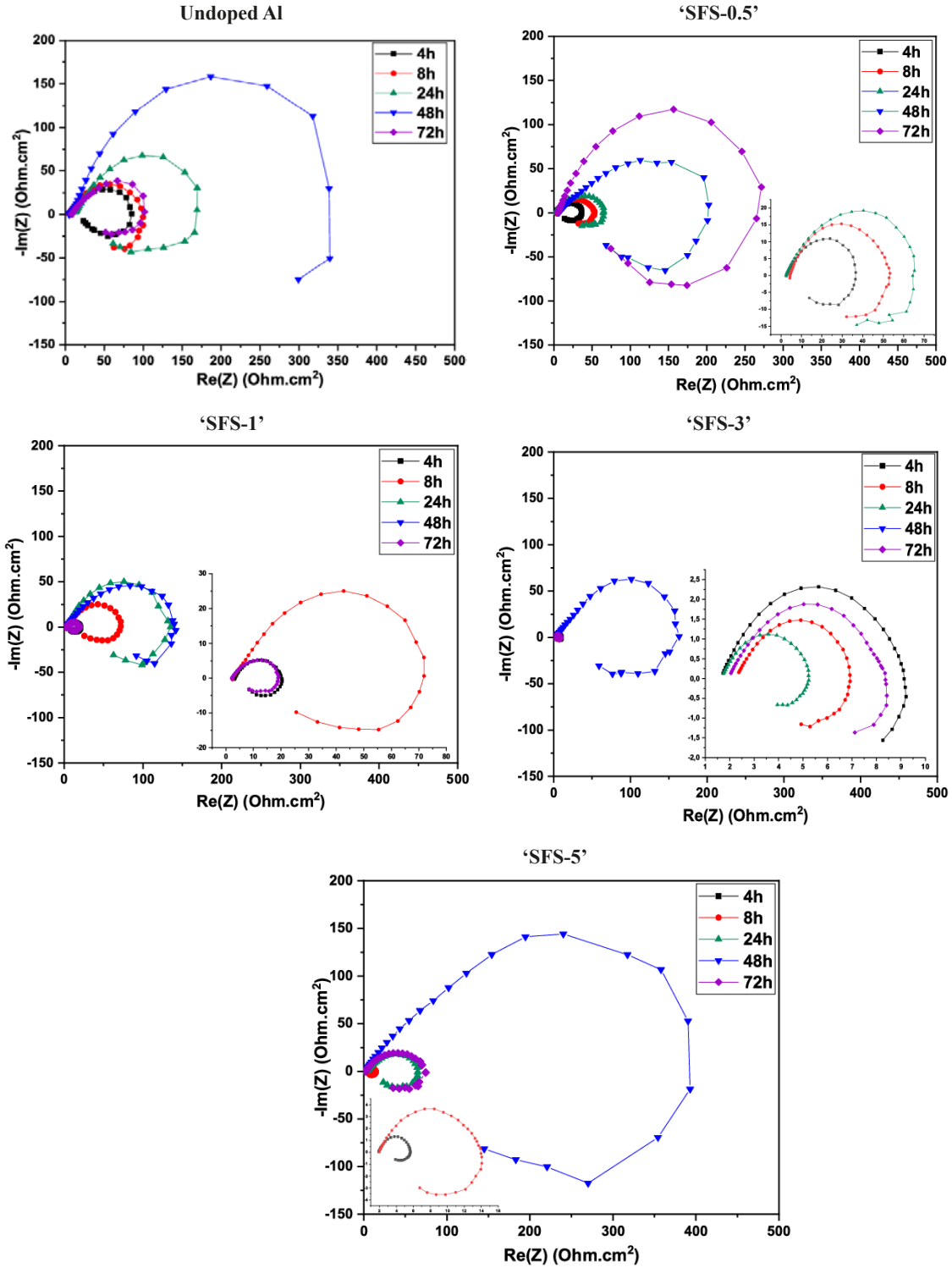

Fig. 3. Nyquist diagrams of undoped aluminum and 'SFS-(0.5, 1, 3, 5)' materials in (1 M) HCl electrolyte in various sintering times at 25°C

The present work explored the impact of the Co composition and the thermal treatment time on the electrochemical impedance performances of undoped aluminum and the'SFS-0.5', 'SFS-1', 'SFS-3', 'SFS-5' materials in acidic medium.

With the addition of Co, there is no change in the shape of the impedance responses. Nevertheless, we observed that the diameter of the Nyquist curves varies according to the dopant composition in all the alloys processed at different sintering times. This indicates that Al doped with cobalt, protects the aluminum corrosion in (1M) HCl medium without modifying the dissolution mechanism of aluminum. In addition, the Nyquist curves shape concords well with what has been reported in the literature [11,12].

The Nyquist diagrams are characterized by two loops: an enormous capacitive loop operating at a high frequency connected to an inductive loop at a low frequency. Most authors attribute the first one to charge transfer mechanisms that happen at the metal/solution interface [11,12,13]. The latter process is mostly based on electron conduction via the surface film or direct electron transfer at the metal surface. Owing to the dielectric properties of the surface layer, this loop is assigned to the transfer resistance assembly with the electrical layer [13]. Whereas the second one has often connected to the surface relaxation or the bulk relaxation of either intermediate product formed on the interface like Cl^{-}, O_2^{-}, H^{+}, or other protected species [11,12]. Moreover, the inductive behavior is more pronounced when these species are strongly absorbed on the interface [11]. A passive film on the aluminum was found to be strongly related to the inductive loop, according to other investigations [14]. Some authors attributed the inductive loop to a quick complementary metal oxidation process, such as $Al^{+} \rightarrow Al^{3+}$, it's based on the redox theory. However, the $Al \rightarrow Al^{+}$ process is related to the actual capacitive response to charge transfer [15].

In Fig. 4, the polarization resistance 'R_p' for the undoped aluminum and the 'SFS-0.5', 'SFS-1', 'SFS-3', and 'SFS-5' materials is depicted for the different thermal treatment times.

At low composition of Co 'SFS-0.5', the polarization resistance 'R_p' increases largely in function of sintering time. However,

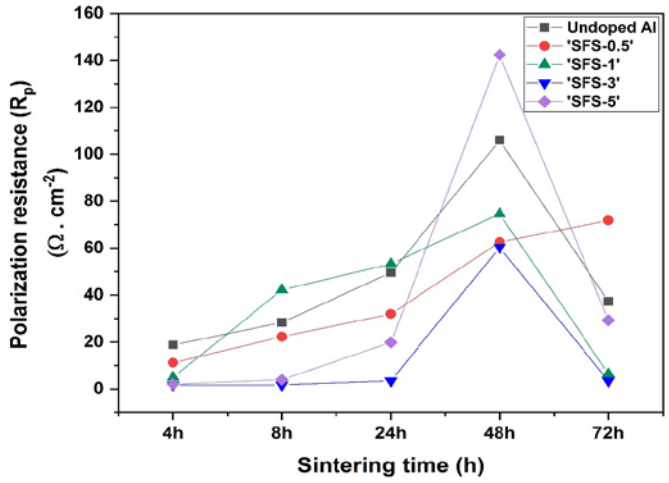

Fig. 4. Polarization resistance 'R_p' development of the undoped Al the 'SFS-0.5', 'SFS-1', 'SFS-3', 'SFS-5' materials at different thermal treatment times in (1 M) HCl electrolyte

a capacitive arc of large diameter starts to increase at the cobalt rate, and sintering time increases in the specimens 'SFS-1', 'SFS-3', and 'SFS-5' and then it decreases. And therefore, the resistance achieved a maximum 'R_p = 142.361' for the 'SFS-5' sample thermally treated at 48 h and which exceeds largely the undoped Al treated again at 48 h. This sintering time remains the optimum time, which represents the highest resistance Rp for these last specimens as shown in (Figs. 3 and 4) and TABLE 2. The increase of R_p could be probably on a drop in the local dielectric constant and/or thickening of the electrical double layer, both of which are primarily brought on by molecular adsorption at the metal/solution interface [11-16].

After this time of thermal treatment '72h', we observed a drop of capacitive arc which may be due to the pores generated by the Kirkendall phenomena [25]. Hence, the effect of the corrosion phenomenon is highly implied.

The increase of polarization resistance is mainly attributed to the reinforcement and the nobility of intermetallic compounds 'Al_9Co_2'and '$Al_{13}Co_4$' on the aluminum matrix (Al). In other manners, the chemical composition, the crystalline structure of precipitates, and their relative quantities are three key elements influencing their corrosion behavior [6-25].

Modeling of the aluminum impedance response and Al-Co alloys in (1 M) HCl medium was accomplished by employing the equivalent circuits depicted in Fig. 5. Ec lab software was employed for the impedance modeling. This model contains a solution resistance (R_s), a series combination of an inductance (L) and inductive resistance (R_L), which is in a parallel position with charge transfer resistance (R_{ct}) and a constant phase element (CPE). When $0 < a < 1$, the impedance response can be described in terms of a CPE for a suitable time-constant distribution. Rather than a perfect condenser (C), it's used to simulate it.

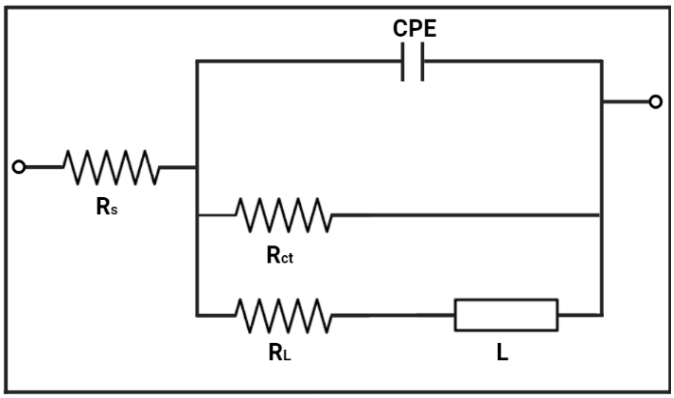

Fig. 5. Impedance spectrum analysis using an electrical equivalent circuil

The results of fitting EIS are given in TABLE 2 and show that cobalt composition and sintering time addition increased the polarization resistance (R_p). The R_p is calculable by the following equation:

$$R_P = \frac{R_{ct} * R_L}{R_{ct} + R_L} \tag{5}$$

TABLE 2

Parameters impedance for undoped Al and Al-Co alloys in (1 M) HCl for various thermal treatment times at 25°C

Specimens	Time	R_s ($\Omega.cm^{-2}$)	CPE_1 ($F.s^{a-1}\ cm^{-2}$)	a_1	R_{ct} ($\Omega.cm^{-2}$)	L ($H.cm^{-2}$)	R_L ($\Omega.cm^{-2}$)	χ^2	R_p
Undoped Al	4 h	7.26±0.29	$1.48e^{-3}$±$0.23e^{-3}$	0.70±0.54	86.04±4.85	134.3±10.16	23.98±0.04	$19.3e^{-2}$	18.75
	8 h	3.92±0.47	$0.95e^{-3}$±$0.13e^{-3}$	0.67±0.53	111.3±4.66	186±14.76	37.97±1.98	$19.7e^{-1}$	28.31
	24 h	11.58±0.34	$2.14e^{-3}$±$0.14e^{-3}$	0.70±0.52	191±8.33	739±31.47	66.95±1.73	$19.0e^{-2}$	49.57
	48 h	5.35±0.27	$2.11e^{-3}$±$0.13e^{-3}$	0.65±0.51	251.2±4.16	299.6±15.16	1613±1064	$27.0e^{-2}$	105.99
	72 h	7.94±0.32	$2.06e^{-3}$±$0.32e^{-3}$	0.64±0.53	120.2±11.68	137.4±15.03	54±1.30	$17.0e^{-2}$	37.26
‘SFS-0.5’	4 h	2.76±0.41	$1.20e^{-3}$±$0.38e^{-3}$	0.66±0.56	35.06±2.03	93.45±11.61	16.36±2.24	$89.2e^{-3}$	11.15
	8 h	4.35±0.35	$0.40e^{-3}$±$80.2e^{-6}$	0.70±0.54	49.02±1.11	333.9±17.7	40.82±6.20	$90.2e^{-3}$	22.27
	24 h	2.34±0.40	$0.79e^{-3}$±$0.12e^{-3}$	0.63±0.53	67.2±2.07	302.1±26.5	60.92±4.75	$60.0e^{-3}$	31.95
	48 h	6.23±0.36	$1.19e^{-3}$±$58.66e^{-6}$	0.53±0.51	246.3±6.56	733.4±22.11	83.89±1.29	$19.0e^{-2}$	62.57
	72 h	5.36±0.30	$0.82e^{-3}$±$37.18e^{-6}$	0.78±0.51	304.3±7.11	742.2±18.36	94.05±1.70	$17.5e^{-2}$	71.84
‘SFS-1’	4 h	3.17±0.38	$0.99e^{-3}$±$0.56e^{-3}$	0.68±0.60	17.11±1.05	87.41±17.44	7.09±1.56	$50.7e^{-3}$	5.01
	8 h	2.66±0.48	$2.52e^{-3}$±$0.47e^{-3}$	0.63±0.54	85.72±7.77	287±30.75	83.26±6.23	$94.5e^{-3}$	42.23
	24 h	2.42±0.30	$1.18e^{-3}$±$96.38e^{-6}$	0.68±0.52	151.7±4.94	484.5±19.76	82.1±2.93	$27.4e^{-2}$	53.27
	48 h	3.19±0.31	$0.85e^{-3}$±$51.9e^{-6}$	0.63±0.51	155.5±2.70	1292±41.94	143.6±5.36	$93.8e^{-3}$	74.65
	72 h	2.26±0.38	$1.81e^{-3}$±$1.01e^{-3}$	0.65±0.60	17.11±1.33	96.15±24.47	10.07±2.05	$99.6e^{-3}$	6.33
‘SFS-3’	4 h	1.71±0.45	$2.67e^{-3}$±$8.50e^{-3}$	0.72±0.92	3.46±1.03	19.24±27.96	3.3±1.86	$47.7e^{-3}$	1.69
	8 h	2.32±0.45	$2.67e^{-3}$±$6.75e^{-3}$	0.71±0.87	4.60±1.24	13.74±11.98	2.76±2.37	$40.5e^{-3}$	1.72
	24 h	1.65±0.45	$1.60e^{-3}$±$2.30e^{-3}$	0.69±0.73	7.61±1.12	41.67±6.76	6.35±6.85	$13.9e^{-3}$	3.46
	48 h	3.03±0.32	$1.40e^{-3}$±$86.8e^{-6}$	0.61±0.51	192.9±6.08	683.5±30.52	87.92±1.51	$32.2e^{-2}$	60.39
	72 h	1.97±0.43	$4.78e^{-3}$±$6.17e^{-3}$	0.64±0.73	6.51±1.09	163±102	7.11±9.17	$14.0e^{-3}$	3.40
‘SFS-5’	4 h	1.93±0.38	$3.76e^{-3}$±0.01	0.77±0.94	3.70±1.03	31.46±50.47	4.40±4.20	$27.2e^{-3}$	2.01
	8 h	1.94±0.38	$1.32e^{-3}$±$1.02e^{-3}$	0.68±0.63	12.08±0.96	89.33±24.22	5.90±2.56	$71.8e^{-3}$	3.96
	24 h	3.55±0.40	$1.55e^{-3}$±$0.23e^{-3}$	0.59±0.531	65.86±2.54	324.9±23.82	28.4±1.90	$86.6e^{-3}$	19.84
	48 h	2.26±0.29	$0.87e^{-3}$±$24.88e^{-6}$	0.60±0.50	502.1±10.64	1404±27.59	198.7±1.66	$16.1e^{-2}$	142.36
	72 h	1.95±0.33	$1.45e^{-3}$±$0.16e^{-3}$	0.60±0.52	74.9±2.13	660.1±40.72	47.98±3.82	$98.2e^{-3}$	29.24

The electrochemical parameters derived from the fitting analysis for aluminum corrosion and its alloys in 1 M HCl are given in TABLE 2. The χ^2 parameter is employed to describe the precision data. All of the specimen’s values are found to be low, indicating that the fitted data and the experimental data concur well. In addition, the lower value ($a = 0.530$) describes a surface inhomogeneity brought on by corrosion products on the surface of the metal [13], and when $a < 1$, the CPE parameter (Q) was attributed to surface heterogeneity [17].

3.3.3. Bode diagrams

The Bode phase angle and Bode modulus diagrams for undoped Al and its alloys in 1 M HCL electrolyte at 25°C are shown in Fig. 6.

In the Bode diagrams, the same shape of all spectra is observed in both cases (the undoped Al and Al-Co alloys). Particularly a middle frequency (MF) and a low frequency (LF) are discernible as two-time constants [12,13] as shown in Fig. 6.

The air-formed layer that covers the macroscopic alloy surface exhibits capacitive behavior, according to the first time constant (MF). The second (LF) was linked to the inductive behavior associated with the surface re-dissolution of the oxide layer or to the relaxing process of species that have been adsorbed in the oxide film that covers the electrode surface [11,12,13].

The increase of the total impedance (phase angle θ and impedance modulus |Z|) with increasing Co content until a sintering time of 48 h could be assigned to one part a reduction in active sites on the aluminum surface. On the other hand, the cobalt adsorption is intensified on the aluminum surface.

The bode parameters are shown in TABLE 3. In the current experiment, the maximum phase angle ‘θ_{max}’ of 34.8093° and the extreme slope ‘S’ value of –0.55062 were found for the ‘SFS-0.5’ alloy treated for 48 hours. The ideal capacitor’s proximity to ‘S’ and ‘θ_{max}’ values reveals the molecules’ adsorption on the surface of the aluminum alloys [31].

3.3.4. Immersion Time Effect

The Nyquist diagram of ‘SFS-5’-48 h is shown in Fig. 7 after immersion in 1 M HCl media for (1, 3, 6, 10, and 15) hours.

The electrical circuit is depicted in Fig. 5. After the simulation of the curve, all collected parameters are grouped in TABLE 4.

According to TABLE 4, the sample ‘SFS-5’-48 had the highest value of polarization resistance „R_p” after 1h. we observe a decrease in this resistance after this time of immersion. This occurs as a result of the metal surface developing a protective double layer. After then, we observe a decline in this layer.

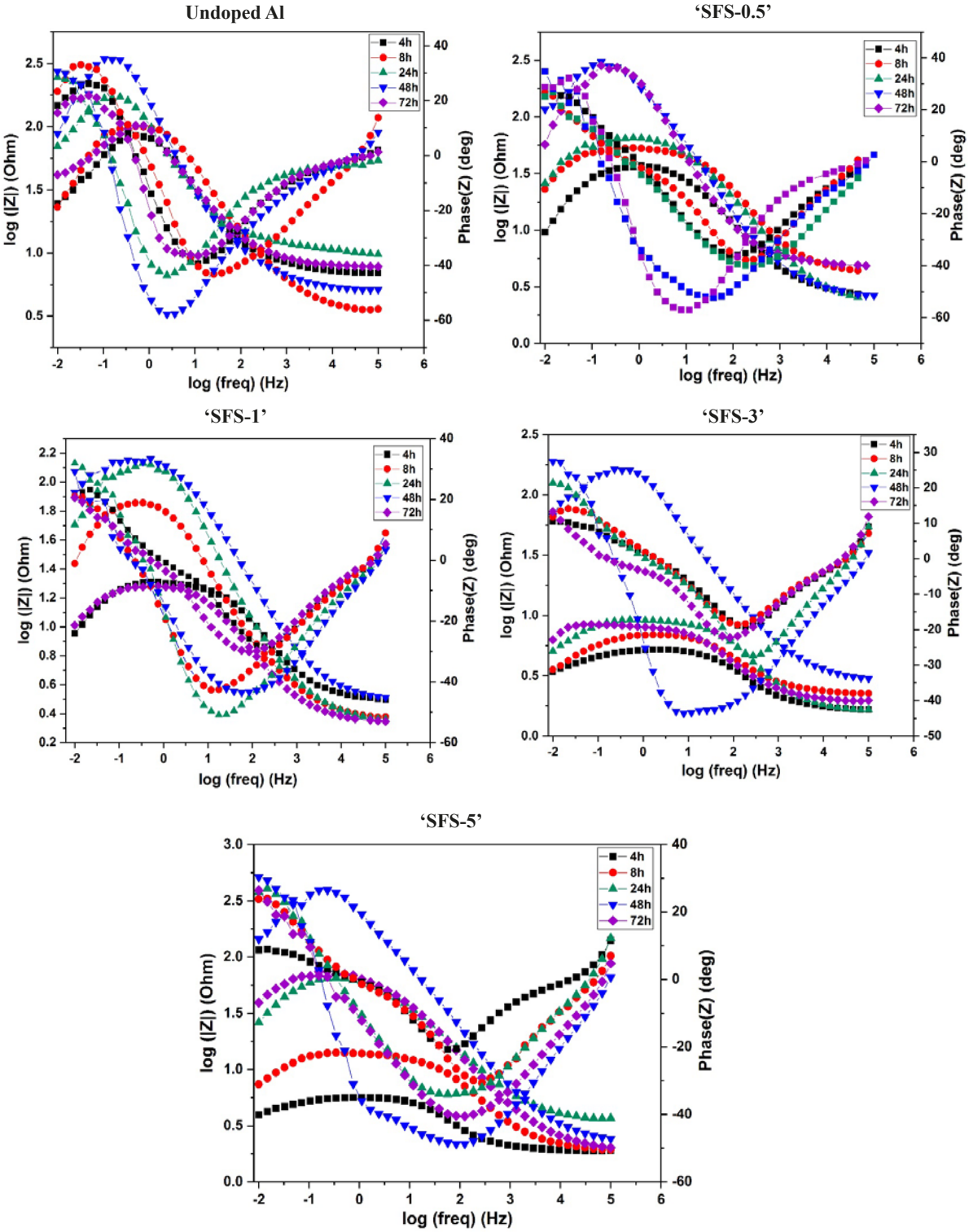

Fig. 6. Bode phase angle (log f vs. $\propto$) and (log f vs. log |Z|) diagrams of impedance plots for the undoped Al and its alloys in 1 M HCl environment

3.4. Surface Identification Film

Fig. 8 shows characteristic Raman spectra of the surfaces for undoped aluminum and its alloys after polarization in an HCl (1M) solution.

Numerous bands make up the Raman spectra, which include: peaks of cobalt oxides/hydroxides, namely CoO, Co_3O_4, and CoOOH [7–21] as well as the alumina hydroxides/oxyhydroxides were found in four primary forms, namely bayerite {–$Al(OH)_3$, boehmite {–AlOOH}, gibbsite {–$Al(OH)_3$} and diaspore {–AlOOH}. According to Raman peaks wavelengths from the bibliography [7,8–18–20], alumina hydrates in their many forms, and cobalt hydroxides and oxides are presented in TABLE 5

The majority of Raman spectra reveal the presence of a broadband starting from 200 cm^{-1} and extending to 550 cm^{-1}.

TABLE 3

Bode settings for the undoped Al and the Al-Co alloys in (1 M) HCl for various thermal treatment times at 25°C

Specimens	Time	θ_{max} (deg)	$Freq_{max}$ (Hz)	Slope (S)
Undoped Al	4 h	26.20	–1.31	–0.42
	8 h	33.03	–1.48	–0.45
	24 h	28.46	–1.99	–0.48
	48 h	30.61	–1.99	–0.58
	72 h	21.85	–1.31	–0.40
'SFS-0.5'	4 h	26.22	–1.82	–0.38
	8 h	26.32	–1.99	–0.41
	24 h	26.76	–1.82	–0.42
	48 h	34.80	–1.99	–0.55
	72 h	32.20	–1.48	–0.61
'SFS-1'	4 h	23.10	–1.65	–0.32
	8 h	20.94	–1.99	–0.44
	24 h	31.91	–1.99	–0.53
	48 h	29.17	–1.99	–0.44
	72 h	20.57	–1.82	–0.31
'SFS-3'	4 h	10.49	–1.99	–0.21
	8 h	14.17	–1.65	–0.20
	24 h	21.32	–1.99	–0.29
	48 h	23.85	–1.65	–0.47
	72 h	13.27	–1.99	–0.23
'SFS-5'	4 h	23.84	–1.99	–0.33
	8 h	26.97	–1.82	–0.36
	24 h	11.62	5.00	–0.22
	48 h	30.38	–1.99	–0.51
	72 h	26.45	–1.99	–0.43

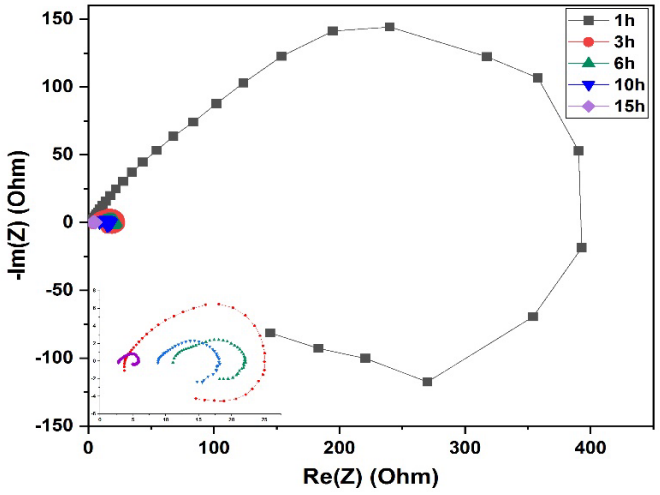

Fig. 7. Nyquist diagram of 'SFS-5'-48 h in 1 M HCl electrolyte at different immersion times

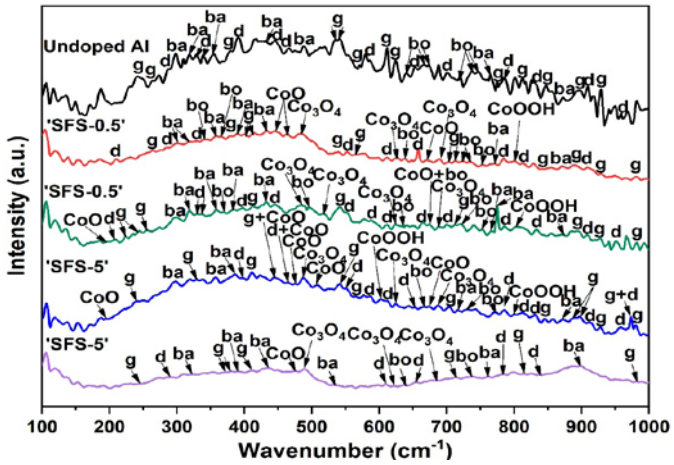

Fig. 8. Raman spectra of undoped Al and 'SFS-0.5' and 'SFS-5' materials sintered at 72 h and 4 h after polarization in (1 M) HCl environment. Aluminum Hydrates: g, gibbsite; d, diaspore; bo, boehmite; bo, pseudoboehmite ba, bayerite. Oxyde and Hydroxyde of Cobalt: CoO, Co_3O_4 and CoOOH

TABLE 4

Electrochemical parameters of 'SFS-5'-48 h in 1 M HCl electrolyte at different immersion times

Samples	Time	R_s ($\Omega.cm^{-2}$)	CPE_1 ($F.s^{a-1}\ cm^{-2}$)	a_1	R_{ct} ($\Omega.cm^{-2}$)	L ($H.cm^{-2}$)	R_L ($\Omega.cm^{-2}$)	χ^2	R_p
'SFS-5'-48 h	1 h	2.26±0.29	$0.87e^{-3}$±$24.88e^{-6}$	0.60±0.50	502.1±10.64	1404±27.59	198.7±1.66	$16.1e^{-2}$	142.36
	3 h	3.75±0.44	$2.69e^{-3}$±$1.14e^{-3}$	0.60±0.58	22.65±1.89	159.8±43.39	19.83±3.24	$84.5e^{-3}$	10.57
	6 h	11.01±0.69	$1.93e^{-3}$±$1.64e^{-3}$	0.5±0.61	11.35±1.37	145.1±73.98	16.61±6.96	$20.9e^{-3}$	6.74
	10 h	8.84±0.52	$2.78e^{-3}$±$2.60e^{-3}$	0.56±0.64	9.49±1.19	143.4±55.2	9.69± 6.95	$11.9e^{-3}$	4.79
	15 h	2.90±0.46	0.02±0.07	0.53±0.91	3.31±2.83	13.18±57.97	6.52± 5.92	$31.3e^{-3}$	2.19

TABLE 5

Raman band wavenumbers of oxide, hydroxide, and oxyhydroxide assignments for the surface layers of undoped Al and its alloys subjected to potentio-static polarization, in (1 M) HCl, at room temperature

	Raman Wavenumbers (cm^{-1})			
Compound	**Al-O**	**γ(OH)**	**δ(OH)**	**References**
Gibbsite γ-$Al(OH)_3$	242,255, 264, 369-372,377-379,398-400, 410-413	537-539, 539-541,569-571, 617, 620, 705-713, 777-779, 814-816,840-845,892, 893-896	924-925,928, 975 979	[7,8–18–20]
Diaspore ∝-AlOOH	207, 287, 328,329, 333-335,394, 466	443-451, 552,583-587, 609,654-658,664, 703-708, 786-790,809-811,832-835,837	909-911,956 975	[7,8–18–20]
Boehmite γ-AlOOH	343-349, 365-369,495	635-636,669-674,721-725, 731*, 731-735, 749-751 (* Pseudoboehmite)	—	[7,8–18–20]
Bayerite ∝-$Al(OH)_3$	296, 318-321, 322-325,358, 387,388-389, 430-432,435, 484, 532-533	716, 764-770,767-771,874-877, 898-899	—	[7,8–18–20]
	F_{2g}	E_g	A_{1g}	References
Co_3O_4	194,617-622	485-488	685-689	[7–21]
CoO	508-510	463-470	672-674	[7]
CoOOH	602-606	—	804-806	[7]

The width of these bands indicates amorphic phase [7–18]. This amorphicity can be attributable to amorphous cobalt oxides or scattered cobalt oxide species [7–27,28]. Beyond a wavenumber superior to 550 cm^{-1}, fine bands characterize the crystallinity of phases above the film surface. Therefore, we can deduce that amorphous and crystalline phases are mixed to form these films. The aluminum surface produces a layer double, an inner layer, and an outer layer. The first one is a compact layer with important amorphously and the second one is a permeable layer of hydrated oxides, which could account for this phenomenon [7–18].

This phenomenon could be explained by the fact that the surface film on aluminum forms a bilayer structure, where the inner layer is a compact amorphous layer while the outer layer is a permeable layer of hydrated oxide [7–18]. The detection of peaks for the aluminum oxyhydroxides/hydroxides and the cobalt oxides/oxyhydroxides is coherent with other works [7–19].

3.5. Microstructure of the corrosion mechanisms

The analysis of microconstituents after polarization was identified by SEM/BSE coupled with EDS. The EDS analysis (Fig. 9(k,l,m)) revealed the presence of intermetallic compounds with different stoichiometries in each phase. This figure provides the sample's microstructure in backscattered electron mode at two magnifications (20 μm and 100 μm). The comparison of the contrasts in BSE mode indicates that light elements backscatter electrons less efficiently than heavy elements. The detection of the phases obtained can be easily distinguished, the less cobalt-rich areas being darker compared to the cobalt-rich areas.

Microstructural examination reveals the manifestation of localized phase corrosion after electrochemical testing in the sample set. Anodic activity occurred in most samples. For undoped aluminum, an aluminum surface is covered by a passive oxide aluminum layer. Pitting and cracks are well highlighted as shown in Fig. 9 (a,b).

In the most negative potentials (TABLE 1), in particular in 'SFS-5' and 'SFS-0.5' materials sintered at 4h (Fig. 9(e,f)) and (Fig. 9(i,j)). When these alloys are attacked by corrosion, the aluminum matrix dissolves preferentially anodically, and pitting in the Al_9Co_2 phase is visible. At 72 h as a shown in Fig. 9(g,h), the 'SFS-5' alloy was sintered, and the same phenomenon was evoked but often the manifestation of a surface partially covered by the alumina film was added to the free Al surface. The oxidation of aluminum is well affected in this alloy which may be responsible for a good corrosion performance compared to the 'SFS-5' material sintered at 4 h (TABLE 1). These observations indicate that the corrosion activity of these alloys can be tailored by the chemical composition.

Since the intermetallic compound, $Al_{13}Co_4$ remains less attacked in the sample set owing to the lack of physical contact between the Al (ss) and $Al_{13}Co_4$ phases [6]. These observations are due to the relative nobility of this microconstituent compared to the intermetallic compound Al_9Co_2 and the aluminum (Al) solid solution. In the Al-Co system, the nobility of the mixed products was compared. The relative amounts of the phases and the physical (and electrical) contacts between them are important for the corrosion performance of the alloy [6–18]. The results indicate that the dissolution of the alloys takes place by a galvanic mechanism. The stability of the alloys depends mainly on the galvanic coupling of less noble phases with phases in chloride media [6]. However, the mixed products of the Al-Co system are brittle [6]. This brittleness can contribute to significant degradation of the alloy through the phenomenon of rapid diffusion [6].

Based on the results, as cobalt composition increases, the nobility of Al-Co binary system intermetallics also does, from the less noble to the nobler phases, in that order.

$$Al\ (ss) < Al_9Co_2 < Al_{13}Co_4 < Al_5Co_2 < \beta\ (Al\ Co)$$

Undoped Al

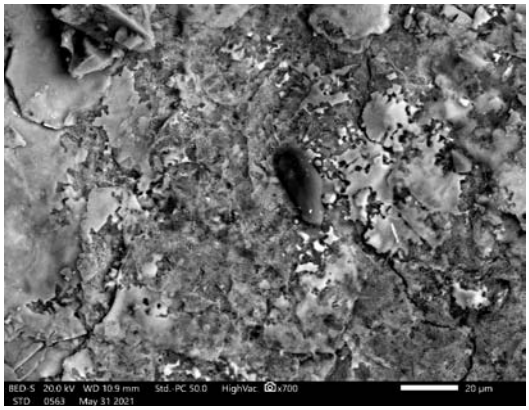

a)

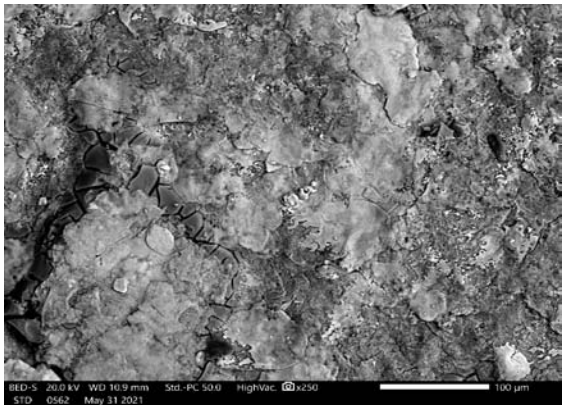

a)

'SFS-5'-72 h

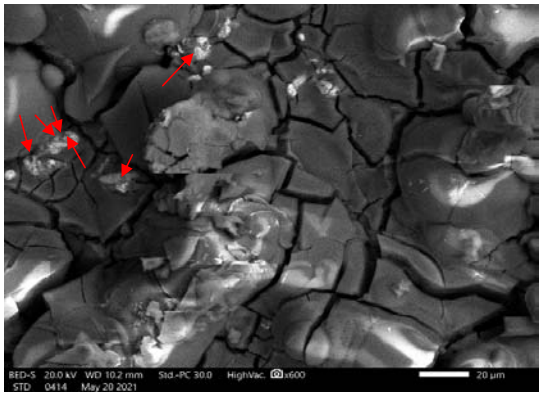

c)

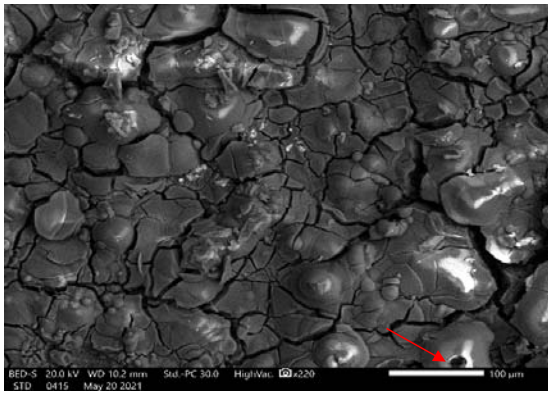

d)

'SFS-5'-4 h

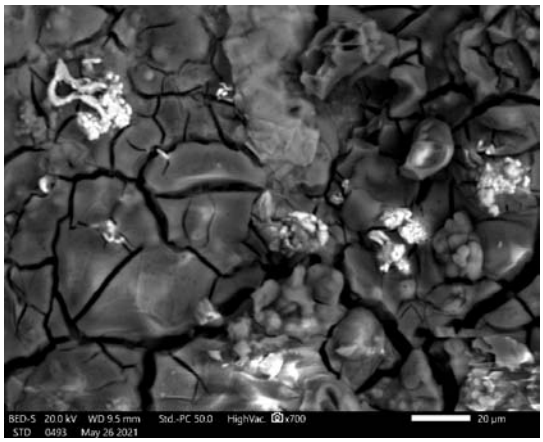

e)

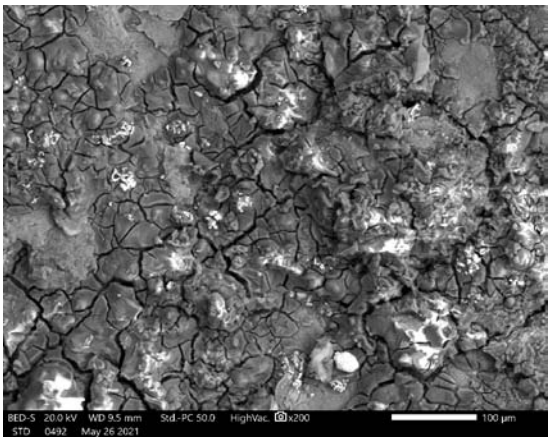

f)

'SFS-0.5'-72 h

g)

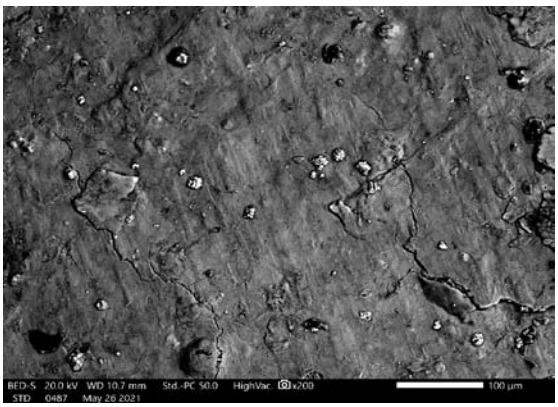

g)

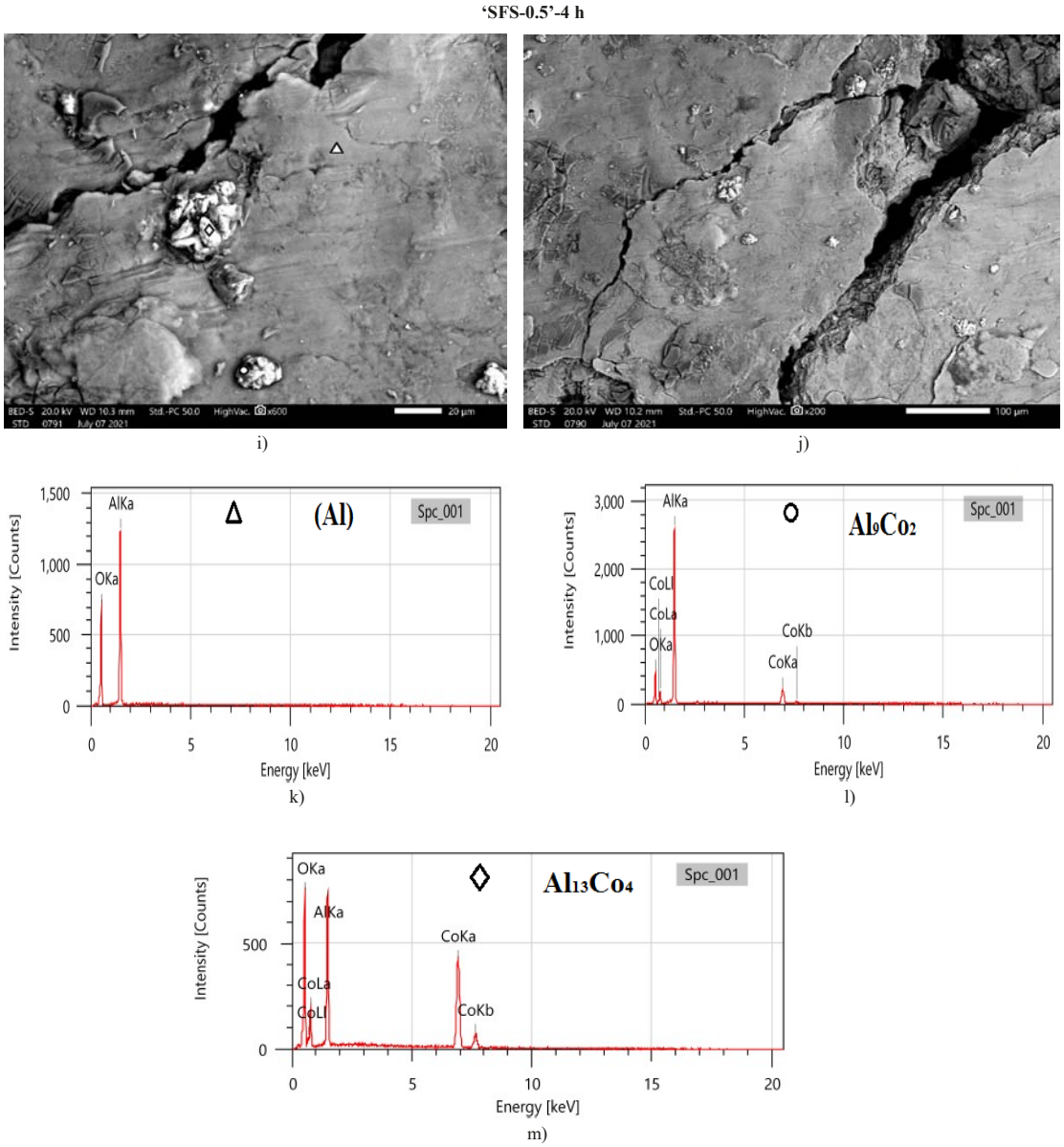

Fig. 9. Microstructure SEM by BSE mode after corrosion testing in HCl medium for the magnifications 20 µm and 100 µm: (a,b) the undoped Al, (c,d;e,f) the 'SFS-5' materials sintered at 72 h and 4 h (g,h;i,j) the'SFS-0.5' materials sintered at 72 h and 4 h, (k,l,m) EDS spectra for each phase

Furthermore, a study showed that the OCP (Open circuit Potential) of Al-Co alloys increases with decreasing pH; meaning that the OCP measured in an alkaline environment was significantly reduced compared to the environment containing chlorides like 'HCl'. This behavior indicates a possible passivation of this material in the aqueous HCl solution [22]. The corrosion performance of these alloys leads to the formation of films covering the surface by:

A passivation of Cobalt into Co oxide and cobalt hydroxide, it is an initially amorphous metal that has higher potentials and is transformed into CoO and Co_3O_4 [18] and a passivation of aluminum into aluminum hydroxides/oxyhydroxides. These films consist of amorphous and crystalline hydrates, as shown in Fig. 9. However, the inherent brittleness of intermetallics leads to fragmentation induced by oxidation processes and dissolution of the adjacent phase (Al) [18]. It can be concluded that the variation of electrochemical parameters depends mainly on several factors which are respectively: chemical composition, sintering time, and structural change.

4. Conclusions

In this study, the electrochemical performance and the microstructure of the undoped Al and the Al-x at.% Co materials with (x = 0.5, 1, 3, and 5) during many sintering cycles (4 h, 8 h, 24 h, 48 h, and 72 h) have been investigated.

The performance corrosion of the materials in (1 M) HCl electrolyte at 25°C was investigated by electrochemical Impedance measurement and Tafel polarization techniques.

The fraction of intermetallic compounds, the amount of cobalt dissolved in the aluminum matrix, and the corrosion

resistance all rose as a consequence of the alloy's increase in Co content. The corrosion resistance is reduced after a certain point in the sintering time, which may be linked to the Kirkendall effects production of porosity.

One characteristic of the intermetallic compounds is the passivation of cobalt and aluminum metals to cobalt and aluminum oxyhydroxides and hydroxides, which display very superior corrosion performance. However, the intermetallic inherent fragility leads to fragmentation brought on by the oxidation and dissolution of the nearby (Al) phase.

It was discovered that each alloy contained a variety of microstructure components. Using an Al-Co phase equilibrium diagram that has already been published, the precipitation sequences of the various phases were established. The electrolyte chloride anions caused the alloys to pit, which was seen. The alloy corrosion performance is influenced by the relative amounts of the phases and the physical (and electrical) contact between them. According to the results, the nobleness of the intermetallics in the Al-Co binary system rises with increasing cobalt content, moving up from lower noble to higher noble products.

REFERENCES

[1] L. Fan, H. Lu, J. Leng , Z. Sun,C. Chen, The Study of Industrial Aluminum Alloy as Anodes for Aluminum-Air Batteries in Alkaline Electrolytes. J. Electrochem. Soc. **163**, A8-A12 (2016). DOI: https://doi.org/10.11 49/2.0021602jes

[2] R.T. Loto, M.M. Solomon, Corrosion Resistance and Passivation Behavior of 3004 AlMnMg and 4044AlSi Aluminum Alloys in Acid-Chloride Electrolytes. Mater. Res. Express. **8**, 096529 (2021). DOI: https://doi.org/10.1088/2053-1591/ac286b

[3] A.M. Abdel-Gaber, B.A. Abd-El-Nabey, I.M. Didahmed, A.M. El-Zayady, M. Saadawy, Kinetics and Thermodynamics of Aluminium Dissolution in 1.0 M Sulphuric Acid containing Chloride Ions. Mater. Chem. Phys. **98**, 291-297 (2006). DOI: https://doi.org/10.1016/j.matchemphys.2005.09.023

[4] N. Chaubey, Savita, V.K. Singh, M.A. Quraishi, Corrosion Inhibition Performance of Different Bark Extracts on Aluminium in Alkaline Solution. J. Assoc. Arab. Univ. Bas. App. Sci. **22**, 38-44 (2017). DOI: https://doi.org/10.1016/j.jaubas.2015.12.003

[5] K. Raviprabha, R.S. Bhat, Electrochemical and Quantum Chemical Studies of 5-[(4-Chlorophenoxy) Methyl]-4H-1,2,4-Triazole-3-Thiol on the Corrosion Inhibition of 6061 Al Alloy in Hydrochloric Acid. J. Fail. Anal. And Preven. **20**, 1598-1608 (2020). DOI: https://doi.org/10.1007/s11668-020-00954-2

[6] M. Palcut, P. Priputen, K. Šalgó, J. Janovec, Phase Constitution and Corrosion Resistance of Al–Co Alloys. Mater. Chem. Phys. **166**, 95-104 (2015). DOI: https://doi.org/10.1016/j.matchemphys.2015.09.032

[7] A.G. Lekatou, A.K. Sfikas, C. Petsa, A.E. Karantzalis, Al-Co Alloys Prepared by Vacuum Arc Melting: Correlating Microstructure Evolution and Aqueous Corrosion Behavior with Co Content. Metals **6**, 46 (2016). DOI: https://doi.org/10.3390/met6030046

[8] A.K. Sfikas, A.G. Lekatou, A.E. Karantzalis, D. Sioulas, Microstructure and Corrosion Behaviour of Aluminium Alloys Containing Complex Metallic Alloy Phases. 3rd International Conference of Engineering Against Fracture (ICEAFIII), Kos, GREECE9, (2013).

[9] A.G. Lekatou, A.K. Sfikas, A.E. Karantzalis, The Influence of the Fabrication Route on the Microstructure and Surface Degradation Properties of Al Reinforced by Al_9Co_2. Mater. Chem. Phys. **200**, 33-49 (2017). DOI: https://doi.org/10.1016/j.matchemphys.2017.07.061

[10] A.S. Fouda, A.A. Al-Sarawy, F.S.H. Ahmed, H.M. El-Abbasy, Corrosion Inhibition of Aluminum 6063 Using Some Pharmaceutical Compounds. Prot. Met. Phys. Chem. Surf. **45**, 635-643 (2009). DOI: https://doi.org/10.1134/S2070205109050244

[11] L.A.L. Guedes, K.G. Bacca, N.F. Lopes, E.M. da Costa, Tannin of Acacia Mearnsii as Green Corrosion Inhibitor for AA7075-T6 Aluminum Alloy in Acidic Medium. Mater. Corros. **70**, 1288-1297 (2019). DOI: https://doi.org/10.1002/maco.201810667

[12] R. Padash, G.S. Sajadi, A.H. Jafari, E. Jamalizadeh, A.S. Rad, Corrosion Control of Aluminum in the Solutions of NaCl, HCl and NaOH using 2,6-dimethylpyridine Inhibitor: Experimental and DFT Insights. Mater. Chem. Phys. **244**, 22681 (2020). DOI: https://doi.org/10.1016/j.matchemphys.2020.122681

[13] N. Chaubey, V.K. Singh, M.A. Quraishi, Papaya Peel Extract as Potential Corrosion Inhibitor for Aluminium alloy in 1 M HCl: Electrochemical and Quantum Chemical Study. Ain. Shams. Eng. J. **9**, 1131-1140 (2018). DOI: https://doi.org/10.1016/j.asej.2016.04.010

[14] H. Hachelef, A. Benmoussat, A. Khelifa, D. Athmani, D. Bouchareb, Study of Corrosion Inhibition by Electrochemical Impedance Spectroscopy Method of 5083 Aluminum Alloy in 1M HCl Solution Containing Propolis Extract. J. Mater. Environ. Sci. **7**, 751-1758 (2016).

[15] M. Stern, A.L. Geary, Electrochemical Polarization, 1. A Theoretical Analysis of the Shape of Polarization Curves. J. Electrochem. Soc. **104**, 56-63 (1975).

[16] D.I. Njoku, I. Ukaga, O.B. Ikenna, E.E. Oguzie, K.L. Oguzie, N. Ibisi, Natural Products for Materials Protection: Corrosion Protection of Aluminium in Hydrochloric Acid by Kola Nitida Extract. J. Mol. Liq. **219**, 417-424 (2016). DOI: https://doi.org/10.1016/j.molliq.2016.03.049

[17] B. Hirschorn, M.E. Orazem, B. Tribollet, V. Vivier, I. Frateur, M. Musiani, Determination of Effective Capacitance and Film Thickness from Constant-Phase-Element Parameters, Electrochimica Acta, **55**, 6218-6227 (2010). DOI: https://doi.org/10.1016/j.electacta.2009.10.065

[18] A.G. Lekatou, A.K. Sfikas, A.E. Karantzalis, D. Sioulas, Microstructure and Corrosion Performance of Al-32%Co alloys. Corros. Sci. **63**, 193-209 (2012). DOI: https://doi.org/10.1016/j.corsci.2012.06.002

[19] S.A. Villaseca, Surfaces d'Alliages Métalliques Complexes à Base d'Aluminium et de Cobalt: Structures Atomique et Electronique. Stabilité et Adsorption, PhD thesis, Lorraine, (2011).

[20] H.D. Ruan, R.L. Frost, J.T. Kloprogge, Comparison of Raman Spectra in Characterizing Gibbsite, Bayerite, Diaspore and Boehmite. J. Raman Spectrosc. **32**, 745-750 (2001). DOI: https://doi.org/10.1002/jrs.736

[21] H. Zhou, L. Chen, V. Malik, C. Knies, D.M. Hofmann, K.P. Bhatti, S. Chaudhary, P.J. Klar, W. Heimbrodt, C. Klingshirn, H. Kalt, Raman studies of ZnO:Co thin films. Phys. Status. Solidi. A. **204**, 112-117 (2007). DOI: https://doi.org/10.1002/pssa.200673019

[22] P. Priputen, M. Palcut, M. Babinec, J. Mišík, I. Černičková, J. Janovec, Correlation Between Microstructure and Corrosion Behavior of Near-Equilibrium Al-Co Alloys in Various Environments. J. Mater. Eng. Perform. **26**, 3970-3976 (2017). DOI: https://doi.org/10.1007/s11665-017-2844-y

[23] A. Yagan, N.O. Pekmez, A. Yildiz, Investigation of Protective Effect of Poly (N-ethylaniline) Coatings on Iron in Various Corrosive Solutions. Surf. Coat. Technol. **201**, 7339-7345 (2007). DOI: https://doi.org/10.1016/ j.surf coat.2007.01.047

[24] G. Palumbo, K. Berent, E. Proniewicz, J. Banas, Guar Gum as an Eco-Friendly Corrosion Inhibitor for Pure Aluminium in 1-M HCl Solution. Materials **12**, 2620 (2019). DOI: https://doi.org/10.3390/ma12162620.

[25] I. Bahaj, M. Kaddami, A. Dahrouch, N. Labjar, M. Essahli, The Effect of Particle Content and Sintering Time on the Properties of Al-Al_9Co_2-$Al_{13}Co_4$ Composites, Made by Powder Metallurgy. Mater. Today : Proc. **62**, A1-A7 (2022). DOI: https://doi.org/10.1016/j.matpr.2022.07.220

[26] A.J. McAlister, The Al-Co (Aluminum-Cobalt) System. Bull. Alloy Phase Diagr. **10**, 646 650 (1989). DOI: https://doi.org/10.1007/BF02877635

[27] J. Tyczkowski, R. Kapica, J. Lojewska, Thin Cobalt Oxide Films for Catalysis Deposited by Plasma-Enhanced Metal-Organic Chemical Vapor Deposition. Thin. Solid. Films. **515**, 6590-6595 (2007). DOI: https://doi.org/10.1016/j.tsf.2006.11.056

[28] M.A. Vuurman, D.J. Stufkens, A. Oskam, G.L. Deo, I.E. Wachs, Combined Raman and IR study of MOx –V_2O_5/Al_2O_3 (MOx = MoO_3, WO_3, NiO, CoO) catalysts under dehydrated conditions. J. Chem. Soc. Faraday Trans. **92**, 3259-3265 (1996). DOI: https://doi.org/10.1039/FT9969203259

[29] I. Bahaj, M. Kaddami, M. Essahli, Elaboration of the Al-Al_3Ni Alloy Eutectic by a Carbothermal Process. Sci. World. J. ID. **7764487**, 12 (2022). DOI: https://doi.org/10.1155/2022/7764487

[30] I. Bahaj, N. Labjar, M. Kaddami, M. Essahli, A. Dahrouch, E. Lotfi, E. Souad, The Influence of Co Content and Sintering Time in Al-Al_9Co_2-$Al_{13}Co_4$ Composites on Microstructure and Corrosion Performance in NaOH Environment. J. Bio. Tribo. Corros. **9**, 4 (2023). DOI: https://doi.org/10.1007/s40735-022-00727-4

[31] M.A. Quraishi, A. Singh, V.K. Singh, D.K. Yadav, A.K. Singh, Green Approach to Corrosion Inhibition of Mild Steel in Hydrochloric Acid and Sulphuric Acid Solutions by the Extract of Murraya Koenigii Leaves. Mater. Chem. Phys. **122**, 114-122 (2010). DOI : https://doi.org/10.1016/j.matchemphys.2010.02.066

[32] S. Diliberto, Elaboration et Caractérisation d'Alliages Réfractaires pour la Fusion du Verre: Alliages Mo WCr, Alliage base Ni "'bi-ODS'". PhD thesis, l'Université Henri Poincaré, Nancy 1 (2000).

[33] S. Aroussi, Elaboration et Caractérisation du Composé NiAl par la Méthode Conventionnelle, SHS et Explosion Thermique. PhD thesis, l' Université Badji Mokhtar-Annaba (2014).